Monthly Notices
of the
ROYAL ASTRONOMICAL SOCIETY

MNRAS **439,** 1940–1947 (2014)
Advance Access publication 2014 February 17

doi:10.1093/mnras/stu087

Torque reversals and pulse profile of the pulsar 4U 1626−67

Aru Beri,[1]★ Chetana Jain,[2] Biswajit Paul[3] and Harsha Raichur[3]

[1]*Department of Physics, Indian Institute of Technology Ropar, Nangal Road, Rupnagar, Punjab 140001, India*
[2]*Hans Raj College, University of Delhi, Delhi 110007, India*
[3]*Raman Research Institute, Sadashivnagar, C. V. Raman Avenue, Bangalore 560 080, India*

Accepted 2014 January 10. Received 2014 January 10; in original form 2013 November 12

ABSTRACT

We review the pulse profile evolution of the unique accretion powered X-ray pulsar 4U 1626−67 over the last 40 yr since its discovery. This pulsar showed two distinct eras of steady spin-up separated by a steady spin-down episode for about 18 yr. In this work, using data from different observatories active during each phase of spin-up and spin-down, we establish a clear correlation between the accretion torque acting on this pulsar and its pulse profile. The energy-resolved pulse profiles are identical in both the spin-up eras and quite different in the spin-down era, especially in the low-energy band. This correlation, along with the already known feature of strong quasi-periodic oscillations (QPO) that was present only in the spin-down era, clearly establishes two different accretion modes on to the neutron star which produce different pulse profiles and only one of which produces the QPOs.

Key words: accretion, accretion discs – pulsars: individual: 4U 1626−67.

1 INTRODUCTION

One of the important manifestations of the interaction between the accretion disc around a neutron star and its magnetic field is the accretion torque on the neutron star, which sometimes results into transitions between spin-up and spin-down of the star. In the standard model of accretion on to magnetized neutron stars, the accretion torque is related to the mass accretion rate on to the neutron star and hence the bolometric X-ray luminosity of the source. Thus, it is expected that the spin transition takes place when the source luminosity decreases below a critical low luminosity which in turn depends on the spin and magnetic moment of the neutron star (Ghosh & Lamb 1979). Transient Be/X-ray binary pulsars and persistent X-ray pulsars which show large X-ray flux variation are therefore ideal sources to verify the standard model of accretion on to high-magnetic-field neutron stars. Many of these sources have shown transitions between spin-up to spin-down and vice versa (Bildsten et al. 1997). However, the torque on to the neutron star and the X-ray luminosity (and therefore mass accretion rate) are not well correlated in either the persistent pulsars with supergiant companions or the low-mass X-ray binary pulsars (Bildsten et al. 1997). Hence, applicability of the standard model of accretion on to the magnetized neutron star is questionable for a large fraction of the X-ray pulsars.

4U 1626−67 is a persistent X-ray source, in which episodes of steady spin-up and spin-down of the pulsar have been observed, and hence is a suitable candidate for a critical examination of the standard model. Unlike most other accreting pulsars, both transient and persistent (Bildsten et al. 1997), transfer of angular momentum is relatively smooth in 4U 1626−67. This source was discovered with the *Uhuru* satellite (Giacconi et al. 1972) and pulsations with a period of ∼7.7 s was discovered with *SAS-3* (Rappaport et al. 1977) and has been observed many times since then. Since its discovery, the pulsar was observed to be spinning up until 1990. One feature that stands out the most in this pulsar is the smooth spin change and occurrence of two torque reversals in a time frame of about 40 yr.

During the first spin-up phase (between 1977 and 1990), observations made with several observatories, like *SAS-3, Einstein, Ginga and EXOSAT*, established a steady spin-up rate of $\sim 8.54 \times 10^{-13}$ Hz s^{-1} (Joss, Avni & Rappaport 1978; Elsner, Ghosh & Lamb 1980; Levine et al. 1988; Shinoda et al. 1990). X-ray luminosity was estimated to be about 1×10^{37} erg s^{-1} (White, Swank & Holt 1983). Chakrabarty et al. (1997) noticed a gradual decrease in X-ray flux during this phase. The pulse profiles analysed using the data of *HEAO* (Pravdo et al. 1979), *TENMA* (Kii et al. 1986) and *EXOSAT* (Levine et al. 1988) showed strong energy dependence. After the torque reversal in 1990, the neutron star in 4U 1626−67 started spinning down at a rate similar in magnitude to the earlier spin-up rate (Chakrabarty et al. 1997). After about 18 yr of steady spin-down, the source again underwent a torque reversal in the beginning of 2008 (Camero-Arranz et al. 2010; Jain, Paul & Dutta 2010). After both the torque reversals, changes in the pulse profile were recorded (Krauss et al. 2007; Jain et al. 2008, 2010). Krauss et al. (2007) also reported a decrease in X-ray flux during this phase. The X-ray flux increased by more than a factor of 2 during the second torque reversal (Camero-Arranz et al. 2010; Jain et al. 2010). During the first spin-up era, weak and broad quasi-periodic oscillations (QPO) at 40 mHz were reported from the *Ginga* observations (Shinoda et al. 1990). However, observations

★ E-mail: aruberi@iitrpr.ac.in

made with *BeppoSAX* (Owens, Oosterbroek & Parmar 1997) and *Rossi X-ray Timing Explorer* (*RXTE*; Kommers, Chakrabarty & Lewin 1998; Chakrabarty 1998) in the spin-down era show strong QPOs at around 48 mHz with a slow frequency evolution with time (Kaur, Paul & Sagar 2008). These 48 mHz QPOs disappeared after the second torque reversal (Jain et al. 2010).

The X-ray spectrum of 4U 1626−67 shows two continuum components: a hard power law and a blackbody. It also shows strong emission lines from oxygen and neon (Angelini et al. 1995; Schulz et al. 2001; Krauss et al. 2007; Camero-Arranz et al. 2012), the strength of which vary with time. In the first spin-up era, the spectrum had a power-law photon index of ∼1.5 and a blackbody temperature of ∼0.6 keV (Pravdo et al. 1979; Kii et al. 1986; Angelini et al. 1995; Vaughan & Kitamoto 1997). In the spin-down era, the energy spectrum became relatively harder with a power-law index of ∼0.4–0.6 and the blackbody temperature decreased to ∼0.3 keV (Angelini et al. 1995; Owens et al. 1997; Vaughan & Kitamoto 1997; Orlandini et al. 1998; Yi & Vishniac 1999). The X-ray spectrum measured with the Proportional Counter Array (PCA) on board *RXTE* (Jain et al. 2010) and *Suzaku* (Camero-Arranz et al. 2012) in the second spin-up phase showed a reversal with a photon index in the range of 0.8–1.0 and a higher blackbody temperature of about 0.5–0.6 keV. The X-ray spectrum in the second spin-up era shows the temperature quite similar to that in the first spin-up era, but the photon index did not return to the same value as that observed during *Phase I* (Angelini et al. 1995; Orlandini et al. 1998; Schulz et al. 2001; Krauss et al. 2007; Camero-Arranz et al. 2010, 2012; Jain et al. 2010). The detection of cyclotron line feature in its spectrum at around 37 keV with several observatories during spin-up and -down phases (Pravdo et al. 1978; Orlandini et al. 1998; Heindl & Chakrabarty 1999; Coburn et al. 2002; Camero-Arranz et al. 2012; Iwakiri et al. 2012) gives a measure of the surface magnetic field of $\sim 3 \times 10^{12}$ Gauss.

In this work, we study the evolution of the pulse profile of 4U 1626−67 during the three phases of accretion torque using data from different observatories. Hereafter, the spin-up era between 1977 and 1990 will be referred to as *Phase I*, spin-down between 1990 and 2008 as *Phase II* and the current era as *Phase III*. The observations made with different observatories in each phase were used to bring out the similarities and/or dissimilarities of the three phases. In the light of our results, we discuss the possible nature and behaviour of torque transfer in this system.

2 OBSERVATIONS, ANALYSIS AND RESULTS

2.1 Representative observations in each phase

For creating the pulse profiles, we analysed one representative long observation in each of the three phases for which archival data are available with sub-second time resolution. The longest observation in *Phase I* was made with *EXOSAT* in 1986 (Levine et al. 1988). Unfortunately, archival data of *EXOSAT* are available only in the form of spectra and light curve with 10 s resolution which are not suitable for the present analysis. Therefore, for *Phase I*, we analysed the longest observation made with the Large Area Counter (LAC) on board *Ginga* observatory (Makino et al. 1987), while for the other two phases the longest observations made with the PCA of the *RXTE* observatory were used (Bradt, Rothschild & Swank 1993). Details of these observations are given in Table 1.

The *Ginga*-LAC covers the energy range of 1.5–37 keV with a photon collection area of 4000 cm^2. Time series from the LAC

Table 1. Log of observations of 4U 1626−67 used in Figs 1–4.

Observatory	Year	Observation ID	Total exposure (ks)
Ginga	1988	880712600	17
RXTE	1996	10101-01-01-00	73
RXTE	2010	95313-01-01-03	32

data was extracted using the tools LACQRDFITS and TIMINFILFITS. Background subtraction from the light curve was done using the Hayashida method.[1] The *RXTE*-PCA consisted of an array of five collimated xenon/methane multi-anode proportional counter units, with a maximum photon collection area of 6500 cm^2 (Jahoda et al. 1996, 2006). PCA data collected in the Good Xenon mode were used to generate the source light curves in the energy band of 2–30 keV. Background light curves in the same energy band were estimated using the tool RUNPCABACKEST assuming a faint source model as suggested by *RXTE* guest observer facility.[2] Thereafter, the photon arrival times in the background-subtracted light curves were corrected to the Solar system barycentre.

2.1.1 *Light curves*

Fig. 1 shows the barycentre-corrected and background-subtracted 2–30 keV light curves in each phase. The plotted light curves have been binned with a bin size of about 10 pulses (77 s). It is obvious from Fig. 1 that flaring events are observed with *Ginga* and *RXTE* detectors during both the spin-up eras. Similar flaring events in both the X-ray and optical data have also been reported earlier (Joss et al. 1978; Li et al. 1980; McClintock et al. 1980; Schulz, Marshall & Chakrabarty 2011). On the other hand, *Phase II* light curve shows lesser variations [also reported by Krauss et al. 2007 using *XMM–Newton* (PN) data].

2.1.2 *Quasi-periodic oscillations*

In Fig. 2, we have shown the power density spectra (PDS) of 4U 1626−67 in the three phases. We have divided the light curves into stretches of 2048 s. PDS from all the segments were averaged to produce the final PDS and were normalized such that their integral gives squared rms fractional variability and the white noise level was subtracted. A strong QPO feature at ∼48 mHz is clearly seen in PDS of *Phase II* data. Presence of strong QPOs in all the *Phase II* observations of this source was reported earlier (Kaur et al. 2008). Absence of the QPOs in *Phase III* and a change in the shape of the PDS from *Phase II* to *Phase III* is already known (Jain et al. 2010). The PDS characteristics in *Phase I* are also different from that in *Phase II*. In only two of the *Phase I* observations QPOs have been observed, with quite different parameters. Kaur et al. (2008) reported the presence of a very narrow QPO in the *EXOSAT*-ME light curve at around 35 mHz, while a weak QPO feature at 40 mHz was seen mainly in the 14–18 keV range of this *Ginga*-LAC observation (Shinoda et al. 1990), which we have reconfirmed.

2.1.3 *Broad-band pulse profiles*

For each of the selected observations in the three phases, we obtained local spin period $P_{\rm spin}$ using the epoch folding χ^2 maximization technique. The pulsar had a $P_{\rm spin}$ of 7.663, 7.6668 and 7.6772 s

[1] http://darts.jaxa.jp/astro/ginga
[2] http://heasarc.gsfc.nasa.gov/docs/xte/pca_news.html

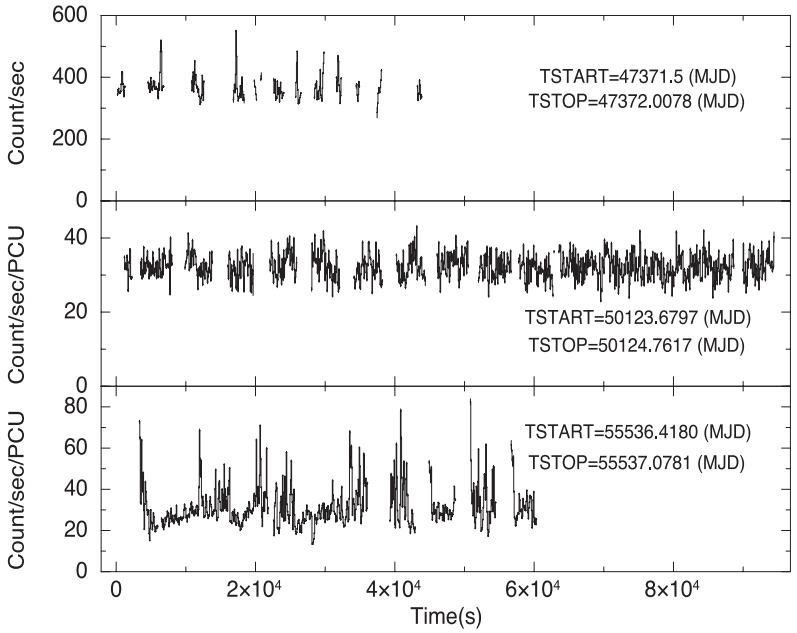

Figure 1. Background-subtracted, barycentre-corrected light curves of 4U 1626−67, obtained from *Ginga* observations, during *Phase I* (top panel) and from *RXTE*-PCA observations during *Phase II* (middle panel) and *Phase III* (bottom panel). X-axis shows time (in seconds) since the beginning of the respective observation. Refer to Table 1 for details.

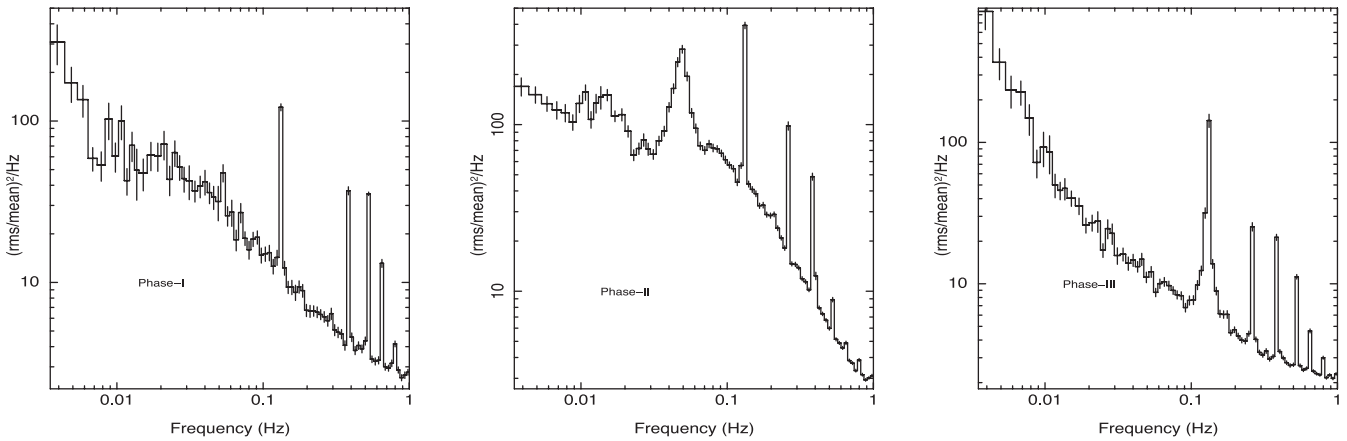

Figure 2. Power spectrum of 4U 1626−67, during the three phase of pulsar spin. From left to right, the power density spectrum of first spin-up, spin-down and second spin-up era are shown, respectively.

during these three observations in *Phase I*, *Phase II* and *Phase III*, respectively. The 2–30 keV light curves were folded at the respective spin periods. Fig. 3 shows the average 2–30 keV pulse profiles, each having 64 phase bins, during the three phases. The pulse profiles have been shifted in pulse phase such that the minimum appears at pulse phase 1.0.

The broad-band pulse profile, as detected using the *Ginga* and *RXTE* data has changed significantly with time. The pulse profile during *Phase I* shows two peaks, with the amplitude of the first peak being slightly more than that of the second peak. The two peaks are separated by a narrow dip and the pulse profile also shows a broad minimum spanning about 0.5 in pulse phase. The *Phase II* pulse profile, on the other hand, does not show the two peaks shown in *Phase I*. The 'broad minimum' feature has also disappeared and the dip is broader and deeper. Two, shallow dips have also appeared at phase 0.4 and 0.7 after the main dip which become broader in *Phase III* pulse profile. The broad-band pulse profile in *Phase III* has features sharper than those in *Phase II* and there is a clear indication of the double-peak feature. The pulse fraction $(I_{\rm max} - I_{\rm min})/I_{\rm max}$ changed from ∼26 per cent during *Phase I* to ∼50 per cent during *Phase II* and ∼44 per cent during *Phase III*. Here, we note that the pulse profile of 4U 1626−67 was measured many times with various observatories in the three phases and in each of the phases, the reported pulse profiles are similar to the profiles shown in Fig. 3 (*Phase I*: Rappaport et al. 1977; Joss et al. 1978; Pravdo et al. 1979; Elsner et al. 1980; Kii et al. 1986; Levine et al. 1988; Mihara 1995; *Phase II*: Angelini et al. 1995; Orlandini et al. 1998; Krauss et al. 2007; Jain et al. 2008, 2010; Iwakiri et al. 2012; *Phase III*: Jain et al. 2010).

2.1.4 *Energy-resolved pulse profiles*

The pulse profile of 4U 1626−67 is known to have strong energy dependence, with a complex pulse shape in the low-energy band

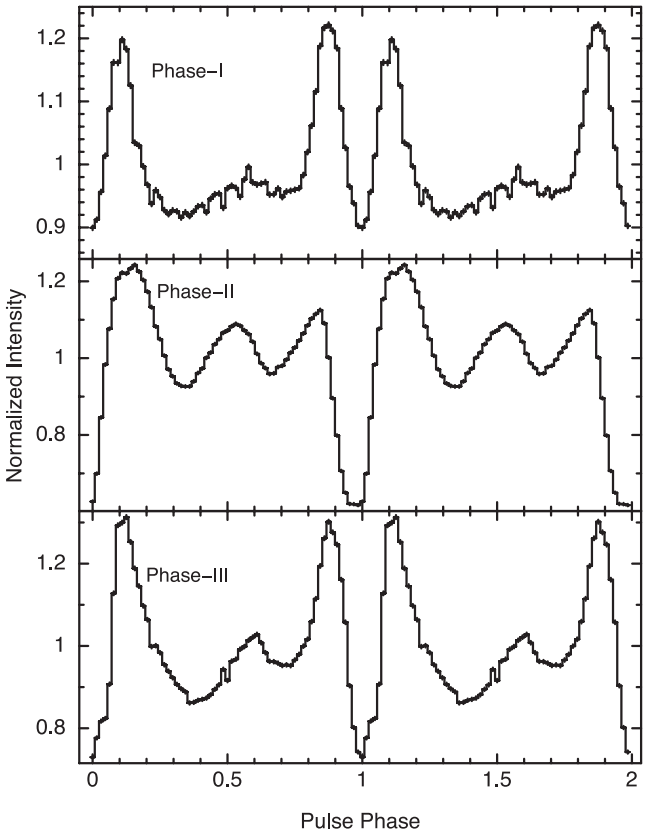

Figure 3. 2–30 keV pulse profile of 4U 1626−67, each divided into 64 phase bins. Top panel: *Ginga* data – *Phase I*, middle panel: *RXTE* data – *Phase II*, bottom panel: *RXTE* data – *Phase III*. The pulse profiles have been shifted in pulse phase such that the minimum appears at pulse phase 1.0.

and a simple broad pulse profile in the high-energy band. Hence, we also compare the pulse profiles in smaller energy bands. The energy-resolved pulse profiles in energy bands of 2–5, 5–8, 8–12, 12–20 and 20–30 keV are shown in Fig. 4. The pulse profiles have many features in the low-energy band and at energies above 20 keV they show a single, broad peak.

The most remarkable feature in Fig. 4 is the difference in the energy-resolved pulse profiles of the two spin-up eras and the spin-down era. The pulse profiles of *Phase I* and *Phase III* across the energy band are quite similar except in the narrow range of 8–12 keV where the pulse profile of *Phase III* bears more resemblance to the respective *Phase II* pulse profile. The feature that stands out the most is the disappearance of the sharp double-peaked pulse profile during spin-down era of *Phase II* and its reappearance in *Phase III*. During the two spin-up eras, with increasing energy, the dips around pulse phase 0.1 broadens and the double peaks disappear. Also, the first of the double peaks in *Phase I* is of greater amplitude than the second peak whereas in *Phase III*, the second peak has greater amplitude than the first peak. In the pulse profile during the spin-down era, there occurs a deep narrow *dip* at low energies which broadens at higher energies.

2.2 Pulse profile history

We further examined similarity between the pulse profiles during the two spin-up eras and differences with the profiles in the spin-down era using all archival data of 4U 1626−67 and the published pulse profiles where archival data or necessary software is not available. We have analysed archival data and created pulse profiles from all the available observations of *RXTE*-PCA during *Phase II* and *Phase III* with exposure time greater than 1000 s. For *Phase II*, we have also analysed data from *ASCA*-GIS (Makishima et al. 1996), *BeppoSAX*-MECS (Boella et al. 1995), *XMM–Newton*-PN (Struder et al. 2001), *Swift*-XRT (Burrows et al. 2005) and *Suzaku*-XIS (Ozawa et al. 2008). Pulse profiles in the energy range of 5–8 keV were created as the characteristic features were prominent and clear in this energy band for most of the observatories. Standard methods, appropriate for the respective instruments, were used for extraction of light curves, estimation and subtraction of background, barycentre correction, pulse period determination and creation of the pulse profile in the 5–8 keV energy band. For the sake of brevity, we do not mention all the details here. For *Phase I*, we have analysed a *Ginga*-LAC observation carried out on 1988 July 29, and for observations with *SAS-3*, *HEAO-1*, *HEAO-2*, *TENMA* and *EXOSAT*-ME, we replotted the published pulse profiles (see references at the end of Section 2.1.3) using the tool *Dexter*.[3]

The pulse profiles of the three spin-up and spin-down eras are shown in Fig. 5 in chronological order. Details of all the observations used for the same are mentioned in Table 2. Since most of the *Phase I* pulse profiles are reproduced from published articles, they are not exactly in the energy range of 5–8 keV. The energy ranges are mentioned in the figure. Within each panel, the pulse phases were aligned to have the minima at the same phase. This figure clearly shows that:

(i) during each of these phases, some lasting more than a decade, the pulse profile in a given energy band remains almost identical.

(ii) the pulse profile in *Phase I* and *Phase III* are quite similar and it is very different in *Phase II*.

(iii) The *Ginga* observation made on 1990 April 19 shows that evolution of the pulse profile started around the period when the spin-down transition began to occur.

3 RESULTS AND DISCUSSION

In this work, we have established a clear correlation between the accretion torque acting on the pulsar 4U 1626−67 and its pulse profile in the three phases of accretion torque. *Phase I* pulse profiles are double peaked and this nature of the pulse profiles disappears in *Phase II* and again reappears in *Phase III*.

In the standard model of accretion on to magnetized compact stars (Ghosh & Lamb 1979), a clear and strong correlation is expected between the mass accretion rate and the accretion torque. A positive correlation between the observed X-ray luminosity and the rate of change of spin period is found in several transient pulsars indicating that, at least in those sources, the observed X-ray luminosity is a measure of the mass accretion rate (Bildsten et al. 1997). At the same time, most of the persistent pulsars do not show a clear correlation between the two quantities. In the case of 4U 1626−67, two abrupt torque reversals between spin-up and spin-down have been detected, associated with significant spectral transition. Apart from the change in the absorption column density, the spectral parameters of the two spin-up phases, *Phase I* and *Phase III*, are similar whereas in *Phase II*, the energy spectrum became relatively harder and the associated blackbody temperature also decreased (Pravdo et al. 1979; Kii et al. 1986; Angelini et al. 1995; Jain et al. 2010; Camero-Arranz et al. 2012). However, during the first

[3] http://dc.zah.uni-heidelberg.de/sdexter

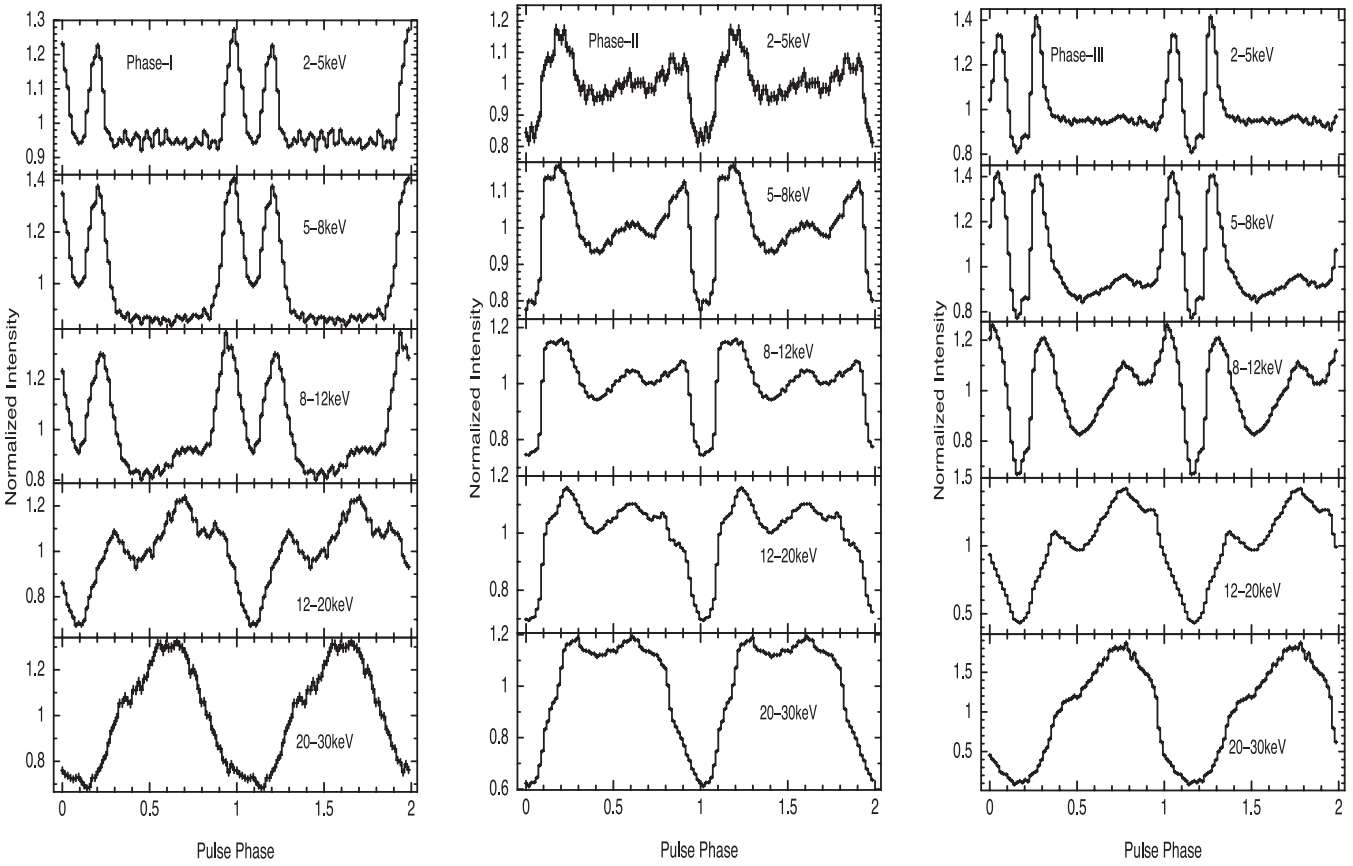

Figure 4. Energy-resolved pulse profile of 4U 1626−67, binned into 64 phase bins. Starting from the top panel, the energy ranges are 2–5, 5–8, 8–12, 12–20 and 20–30 keV. The first set of panels on the left are from *Ginga* observations, while the other two are from *RXTE* observations.

torque reversal (from spin-up to spin-down), the X-ray flux had been decreasing monotonically (Angelini et al. 1995; Owens et al. 1997; Krauss et al. 2007). This decrease is insignificant on short time-scales near the reversal and hence insufficient to explain the sudden change of accretion torque. The second torque reversal (from spin-down to spin-up) was also abrupt, but it was accompanied by an increase in the X-ray flux (Camero-Arranz et al. 2010; Jain et al. 2010). During the entire *Phase II*, the X-ray flux decreased which was associated with only a small change in the spin-down rate (Krauss et al. 2007). Thus, a detailed comparison of the long-term X-ray flux history and the spin history implies that if the X-ray luminosity is proportional to the mass accretion rate, then mass accretion rate is not the sole criteria affecting the transfer of torque in this system.

In addition to the shape of the energy-dependent pulse profile, we have found several other similarities of the source character in the two spin-up phases. Strong flares are seen only in *Phase I* and *Phase III* and not in *Phase II*. The PDS has a power-law shape and the QPOs are absent/weak in *Phase I* and *Phase III* which is contrary to its character in *Phase II* (Jain et al. 2010).

Based on the changes in the pulse profile, Krauss et al. (2007) had earlier proposed a change in the accretion mode during the first torque reversal. Jain et al. (2010) had proposed a change in the accretion mode during the second torque reversal mainly based on the change in the shape of the PDS and disappearance of the QPOs in *Phase III*.

Energy-dependent dips are known in many X-ray pulsars. Dip features that are prominent in the low-energy band and disappear above about 7–15 keV are explained to be due to absorption in the phase-locked accretion streams (Devasia et al. 2011; Maitra, Paul & Naik 2012). The low-energy pulse profiles of 4U 1626−67 can also be explained in a similar way if there is a strong, narrow, soft emission component from the polar hotspot, the peak of which is strongly absorbed by the same accretion stream that produces the hotspot, giving rise to the dip feature. In the *Phases I* and *III*, the absorbing structure is narrower than the emission beam resulting in two peaks while in *Phase II*, the accretion stream absorbs most of the hotspot emission. It is possible that there is another emission component that has a broad pulse profile and dominates in the high-energy band, >20 keV. The high-energy component does not vary very much in the different phases, but the strength of the emission from the hotspot and the strength of the absorption by the accretion stream varies, the absorption being stronger in *Phase II*.

The above scenario requires the size and shape of the polar hotspot regions and the geometry of the accretion stream to be different in the different *phases* of 4U 1626−67. Accretion from the inner disc to the neutron star surface probably happens in different modes that are steady over many years. Transitions between such stable accretion states with different geometry of the accretion flow can give rise to different X-ray spectra and pulse profiles as observed in 4U 1626−67. An interesting possibility is a radiation-pressure-induced warping of the inner accretion disc which may become retrograde leading to negative accretion torque of similar magnitude (van Kerkwijk et al. 1998). The same authors have also pointed out that what sets the time-scale for such transitions in different sources is not clear. While the QPO features may be different

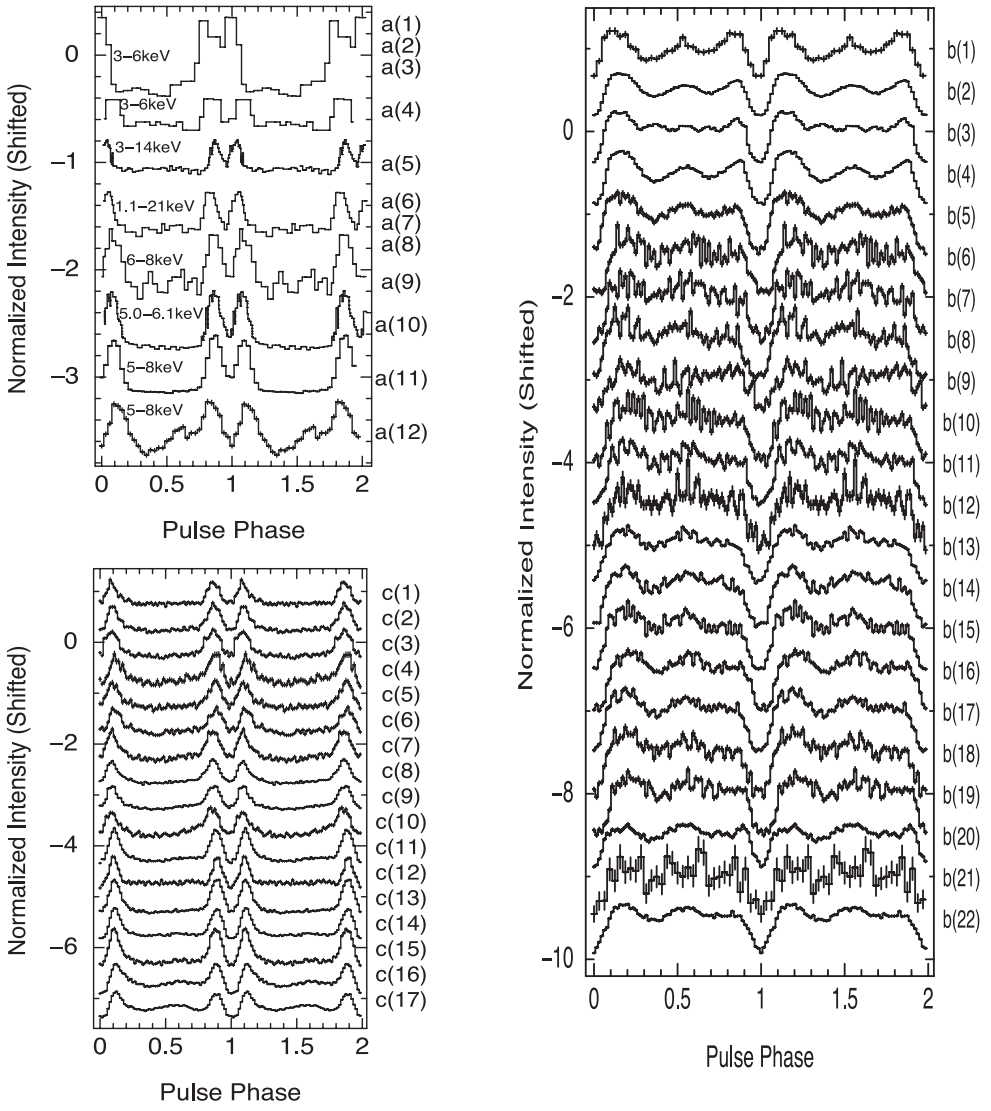

Figure 5. Pulse profiles of 4U 1626−67 using all the available observations in each of the three phases in the energy range of 5–8 keV, each vertically shifted for ease of viewing. The three panels clockwise from top-left are for the three phases I, II and III, respectively.

in different accretion states, it is also to be noted that there are fewer flares in the spin-down era.

A change in accretion mode in *Phase II* compared to the other two phases can also result into the observed energy-dependent pulse profiles in the following manner. In the two spin-up eras, there may be a steady accretion column formed which feeds the neutron star at a constant mass accretion rate. This accretion column intercepts the emission cone such as to form the narrow dips seen between the double peaks. During *Phase II*, the accretion is probably from a more clumpy material roughly forming an accretion column which manifests itself with pulse-phase-dependent variation in the absorption column density explaining the increase in the number of features in the average pulse profile. This may also explain the presence of QPOs during *Phase II* if we assume that QPOs are a manifestation of clumps in the inner accretion disc.

We also note here some other possibilities that were pointed out earlier to explain the torque reversals in 4U 1626−67 and some associated characteristics. Nelson et al. (1997) had proposed that a transition between prograde and retrograde discs causes the torque reversal in 4U 1626−67. While formation of a retrograde disc is quite possible in wind-fed systems, in the case of Roche lobe overflow systems the possibility of a retrograde disc formation and it being present for an extended period is not certain. Switching between Keplerian and sub-Keplerian rotation of the accretion flow (Narayan & Yi 1995; Yi & Vishniac 1999) was also proposed to be a reason for the change of state. In this work, we have given strong observational evidences for a change in the accretion mode during the torque reversals, which is possibly in the form of changes in the accretion flow geometry from the inner part of the accretion disc to the neutron star.

ACKNOWLEDGEMENTS

We would like to thank all the members of *Ginga* for their support in the software installation. This research has made use of data obtained from the Data ARchives and Transmission System (DARTS) and High Energy Astrophysics Science Archive Research Center (HEASARC), provided by NASA's Goddard Space Flight Center.

Table 2. Observations used for the study of profile history of 4U 1626−67.

Phase	Observatory	Date of observation and profile number	
	SAS-3	1977-03-24	a(1)
	SAS-3	1977-03-25	a(2)
	SAS-3	1977-03-26	a(3)
	SAS-3	1978-05-30	a(4)
	HEAO-I	1978-03-29	a(5)
Phase I	*HEAO-2*	1979-02-24	a(6)
	HEAO-2	1979-03-10	a(7)
	HEAO-2	1979-03-14	a(8)
	Tenma	1983-05-03	a(9)
	EXOSAT	1986-03-30	a(10)
	Ginga	1988-07-29	a(11)
	Ginga	1990-04-19	a(12)
	ASCA-GIS	1993-08-11	b(1)
	RXTE-PCA	1996-02-10	b(2)
	RXTE-PCA	1996-02-13	b(3)
	RXTE-PCA	1996-02-14	b(4)
	BeppoSAX-MECS	1996-08-09	b(5)
	RXTE-PCA	1996-12-25	b(6)
	RXTE-PCA	1997-05-11	b(7)
	RXTE-PCA	1997-06-10	b(8)
	RXTE-PCA	1997-07-17	b(9)
	RXTE-PCA	1997-11-17	b(10)
Phase II	*RXTE*-PCA	1997-12-13	b(11)
	RXTE-PCA	1998-06-25	b(12)
	RXTE-PCA	1998-06-27	b(13)
	RXTE-PCA	1998-06-27	b(14)
	RXTE-PCA	1998-06-28	b(15)
	RXTE-PCA	1998-06-29	b(16)
	RXTE-PCA	1998-07-26	b(17)
	RXTE-PCA	1998-07-27	b(18)
	RXTE-PCA	1998-07-27	b(19)
	XMM-PN	2003-08-20	b(20)
	Swift-XRT	2006-02-15	b(21)
	Suzaku-XIS	2006-03-09	b(22)
	RXTE-PCA	2009-06-02	c(1)
	RXTE-PCA	2009-06-02	c(2)
	RXTE-PCA	2009-06-03	c(3)
	RXTE-PCA	2010-01-14	c(4)
	RXTE-PCA	2010-01-14	c(5)
	RXTE-PCA	2010-01-14	c(6)
	RXTE-PCA	2010-01-14	c(7)
	RXTE-PCA	2010-01-14	c(8)
	RXTE-PCA	2010-01-15	c(9)
Phase III	*RXTE*-PCA	2010-01-15	c(10)
	RXTE-PCA	2010-12-04	c(11)
	RXTE-PCA	2010-12-04	c(12)
	RXTE-PCA	2010-12-04	c(13)
	RXTE-PCA	2010-12-06	c(14)
	RXTE-PCA	2010-12-06	c(15)
	RXTE-PCA	2010-12-07	c(16)
	RXTE-PCA	2010-12-09	c(17)

REFERENCES

Angelini L., White N. E., Nagase F., Kallman T. R., Yoshida A., Takeshima T., Becker C., Paerels F., 1995, ApJ, 449, L41

Bildsten L. et al., 1997, ApJS, 113, 367

Boella G. et al., 1995, Proc. SPIE, 2517, 223

Bradt H. V., Rothschild R. E., Swank J. H., 1993, A&AS, 97, 1

Burrows D. N. et al., 2005, Space Sci. Rev., 120, 165

Camero-Arranz A., Finger M. H., Ikhsanov N. R., Wilson-Hodge C. A., Beklen E., 2010, ApJ, 708, 1500

Camero-Arranz A., Pottschmidt K., Finger M. H., Ikhsanov N. R., Wilson-Hodge C. A., Marcu D. M., 2012, A&A, 546, 40

Chakrabarty D., 1998, ApJ, 492, 342

Chakrabarty D. et al., 1997, ApJ, 474, 414

Coburn W., Heindl W. A., Rothschild R. E., Gruber D. E., Kreykenbohm I., Wilms J., Krteschmar P., Staubert R., 2002, ApJ, 580, 394

Devasia J., James M., Paul B., Indulekha K., 2011, MNRAS, 417, 348

Elsner R. F., Ghosh P., Lamb F. K., 1980, ApJ, 241, L155

Ghosh P., Lamb F. K., 1979, ApJ, 234, 296

Giacconi R., Murray S., Gursky H., Kellogg E., Schreier E., Tananbaum H., 1972, ApJ, 178, 281
Heindl W. A., Chakrabarty D., 1999, in Aschenbach B., Freyberg M. J., eds, Highlights in X-ray Astronomy. MPE, Garching, p. 25
Iwakiri W. B. et al., 2012, ApJ, 751, 35
Jahoda K., Swank J. H., Giles A. B., Stark M. J., Strohmayer T., Zhang W., Morgan E. H., 1996, Proc. SPIE, 2808, 59
Jahoda K., Markwardt C. B., Radeva Y., Rots A. H., Stark M. J., Swank J. H., Strohmayer T. E., Zhang W., 2006, ApJS, 163, 401
Jain C., Paul B., Dutta A., Joshi K., Raichur H., 2008, J. Astrophys. Astron., 28, 175
Jain C., Paul B., Dutta A., 2010, MNRAS, 403, 920
Joss P. C., Avni Y., Rappaport S., 1978, ApJ, 221, 645
Kaur R., Paul B., Sagar R., 2008, ApJ, 676, 1184
Kii T., Hayakawa S., Nagase F., Ikegami T., Kawai N., 1986, PASJ, 38, 751
Kommers J. M., Chakrabarty D., Lewin W. H. G., 1998, ApJ, 497, L33
Krauss M. I., Schulz N. S., Chakrabarty D., Juett A. M., Cottam J., 2007, ApJ, 660, 605
Levine A., Ma C. P., McClintock J., Rappaport S., van der Klis M., Verbunt F., 1988, ApJ, 327, 732
Li F. K., McClintock J. E., Rappaport S., Wright E. L., Joss P. C., 1980, ApJ, 240, 628
McClintock J. E., Li F. K., Canizares C. R., Grindlay J. E., 1980, ApJ, 235, L81
Maitra C., Paul B., Naik S., 2012, MNRAS, 420, 2307
Makino F., Astro-C team, 1987, Astrophys. Lett. Commun., 25, 223
Makishima K. Astro-D team, 1996, PASJ, 48, 171
Mihara T., 1995, PhD thesis, Univ. Tokyo
Narayan R., Yi I., 1995, ApJ, 452, 71
Nelson R. W. et al., 1997, ApJ, 488, L117
Orlandini M. et al., 1998, ApJ, 500, L163
Owens A., Oosterbroek T., Parmar A. N., 1997, A&A, 324, L9
Ozawa M. et al., 2008, in Turner M. J. L., Flanagan K. A., eds, Proc. SPIE Conf. Ser. Vol. 7011, Space Telescopes and Instrumentation 2008: Ultraviolet to Gamma Ray. SPIE, Bellingham, p. 70112B
Pravdo S. H., Bussard R. W., Becker R. H., Boldt E. A., Holt S. S., Serlemitsos P. J., 1978, ApJ, 225, 988
Pravdo S. H. et al., 1979, ApJ, 231, 912
Rappaport S., Markert T., Li F. K., Clark G. W., Jernigan J. G., McClintock J. E., 1977, ApJ, 217, L29
Schulz N. S., Chakrabarty D., Marshall H. L., Canizares C. R., Lee J. C., Houck J., 2001, ApJ, 563, 941
Schulz N. S., Marshall H. L., Chakrabarty D., 2011, Am. Astron. Soc. Meeting Abstr., 218, 122.05
Shinoda K., Kii T., Mitsuda K., Nagase F., Tanaka Y., Makishima K., Shibazaki N., 1990, PASJ, 42, L27
Struder L. et al., 2001, A&A, 365, L18
van Kerkwijk M. H., Chakrabarty D., Pringle J. E., Wijers R. A. M. J., 1998, ApJ, 499, L27
Vaughan B. A., Kitamoto S., 1997, preprint (arXiv:astro-ph/9707105)
White N. E., Swank J. H., Holt S. S., 1983, ApJ, 270, 711
Yi I., Vishniac E. T., 1999, ApJ, 516, L87

This paper has been typeset from a TEX/LATEX file prepared by the author.